Evaluation of F8-TNF- in Models of Early and Progressive Metastatic Osteosarcoma

Robl, Bernhard ; Botter, Sander Martijn ; Boro, Aleksandar ; Meier, Daniela ; Neri, Dario ; Fuchs, Bruno

DOI: https://doi.org/10.1016/j.tranon.2017.02.005

Translational Oncology
www.transonc.com

Volume 10 Number 3 June 2017 pp. 419–430 419

Evaluation of F8-TNF-α in Models of Early and Progressive Metastatic Osteosarcoma[1]

Bernhard Robl*, Sander Martijn Botter*, Aleksandar Boro*, Daniela Meier*, Dario Neri† and Bruno Fuchs*

*Laboratory for Orthopedic Research, Department of Orthopedics, Balgrist University Hospital, Zurich, Switzerland; †Institute of Pharmaceutical Sciences, ETH Zurich, Zurich, Switzerland

Abstract

The targeted delivery of tumor necrosis factor-α (TNF-α) with antibodies specific to splice isoforms of fibronectin [e.g., F8-TNF, specific to the extra-domain A (EDA) domain of fibronectin] has already shown efficacy against experimental sarcomas but has not yet been investigated in orthotopic sarcomas. Here, we investigated F8-TNF in a syngeneic K7 M2–derived orthotopic model of osteosarcoma as a treatment against pulmonary metastases, the most frequent cause of osteosarcoma-related death. Immunofluorescence on human osteosarcoma tissue confirmed the presence of EDA in primary tumors (PTs) as well as metastases. In mice, the efficacy of F8-TNF against PTs and early pulmonary metastases was evaluated. Intratibial PT growth was not affected by F8-TNF, yet early micrometastases were reduced possibly due to an F8-TNF–dependent attraction of pulmonary $CD4^+$, $CD8^+$, and natural killer cells. Furthermore, immunofluorescence revealed stronger expression of EDA in early pulmonary metastases compared with PT tissue. To study progressing pulmonary metastases, a hind limb amputation model was established, and the efficacy of F8-TNF, alone or combined with doxorubicin, was investigated. Despite the presence of EDA in metastases, no inhibition of progressive metastatic growth was detected. No significant differences in numbers of $CD4^+$ or $CD8^+$ cells or $F4/80^+$ and $Ly6G^+$ myeloid-derived cells were observed, although a strong association between metastatic growth and presence of pulmonary $Ly6G^+$ myeloid-derived cells was detected. In summary, these findings demonstrate the potential of F8-TNF in activating the immune system and reducing early metastatic growth yet suggest a lack of efficacy of F8-TNF alone or combined with doxorubicin against progressing osteosarcoma metastases.

Translational Oncology (2017) 10, 419–430

Introduction

Primary bone cancers, with osteosarcoma as its most common representative, are among the deadliest cancers in children and adolescents [1,2]. Following the introduction of chemotherapy in the 1970s, 5-year survival rates of osteosarcoma increased significantly except for patients with metastatic disease, which remained at a low 20% until today [3]. Although the primary tumor (PT) can be effectively treated using modern multidrug chemotherapy schemes [i.e., doxorubicin (DOX), methotrexate, cisplatin] and surgery, metastatic disease is inefficiently treated and thus remains to be the strongest prognostic factor for poor patient survival [4].

To date, several studies demonstrated improved survival rates of osteosarcoma patients after standard chemotherapy if hallmarks of an activated immune system are present. For instance, postoperative

Address all correspondence to: Prof. Bruno Fuchs, MD, PhD, Laboratory for Orthopedic Research, Department of Orthopedics, Balgrist University Hospital, Forchstrasse 340, 8008, Zurich, Switzerland. E-mail: bruno.fuchs@uzh.ch

[1] Funding; This work was supported by the University of Zurich, the Schweizerischer Verein Balgrist (Zurich, Switzerland), the Walter L. & Johanna Wolf Foundation (Zurich, Switzerland), the Highly Specialized Medicine for Musculoskeletal Oncology program of the Canton of Zurich, the Zurcher Krebsliga (Zurich, Switzerland), the "Kind und Krebs" fund (Zollikerberg, Switzerland), the ERC (Advanced Grant "ZAUBERKUGEL"), and the Swiss National Science Foundation (SNF Nr. 310030_149649).
Received 9 January 2017; Revised 16 February 2017; Accepted 16 February 2017

1936-5233/17
http://dx.doi.org/10.1016/j.tranon.2017.02.005

infections in nonmetastatic osteosarcoma patients [5] as well as a high ratio of intratumoral $CD8^+/FOXP3^+$ lymphocytes [6] were found to be prognostic for improved survival rates of osteosarcoma patients. In addition to improved survival rates, early recovery of lymphocytes after neoadjuvant chemotherapy was indicative for fewer relapses and was even observed to control metastatic disease [7]. Similarly, a higher presurgical lymphocytes to monocytes ratio was associated with better survival rates as well as a lower frequency of metastases at diagnosis [8]. The addition of liposomal muramyl tripeptide phosphatidylethanolamine, a stimulator of innate immunity, to standard chemotherapy also demonstrated significantly improved overall survival rates of osteosarcoma patients [9]. Taken together, these studies point to a survival benefit for osteosarcoma patients mediated through a competent immune system. Thus, it will be important to find out how to further potentiate an effective anticancer immune response.

Already established cytotoxic chemotherapeutics such as anthracyclines (e.g., DOX) can also induce immunogenic cell death [10]. To further enhance this chemotherapy-induced immune response, a potent immunostimulatory cytokine can be employed. One of the most potent proinflammatory cytokines is tumor necrosis factor–α (TNF-α). Already around 1900, TNF-α contributed to impressive antitumor effects against sarcomas and lymphomas [11,12]. The antitumor effects of TNF-α depend on the tumor-bearing host [13], especially its immune activating properties [14,15] or destruction of the tumor vasculature [15,16]. However, systemic use of TNF-α is limited through severe cytotoxic side effects leading to shock, tissue injury, and even death, already observed at TNF-α levels which can endogenously be produced by the host [17]. To overcome limiting toxicities and to locally enhance therapeutic effects, various targeting moieties (e.g., NGR-containing peptides, or the F8, L19, TCP-1 antibodies) have previously been coupled to TNF-α, with the aim of guiding it to specific domains present in the tumor vasculature [18–21]. For instance, TNF-α linked to the F8-moiety (F8-TNF), which targets the extra-domain A (EDA) of fibronectin, was already demonstrated to have strong therapeutic efficacy against established subcutaneous (s.c.) soft tissue sarcomas [19]. Furthermore, locally increased drug concentrations of F8-TNF may further enhance its efficacy. In osteosarcoma patients, intratumoral concentrations of standard chemotherapeutics (e.g., cisplatin) were elevated if the drug was directly infused via the tumor feeding artery as compared with standard intravenous (i.v.) administrations [22]. Recently, we demonstrated that local intraarterial (i.a.) infusions of cisplatin indeed led to superior tumor control [23].

In this study, we investigated the potential of F8-TNF to control primary osteosarcoma growth as well as systemic spread and metastatic disease. Using a clinically relevant syngeneic K7 M2–derived orthotopic mouse model of osteosarcoma, drug efficacy was first evaluated in early metastatic disease and in dependence of its route of administration (i.e., i.a. versus i.v.). Because of the limited time available for development of metastases, a hind limb amputation model as previously described by Wolfe et al. was established [24]. This model allowed the development and monitoring of late metastatic growth and was subsequently used to test the efficacy of F8-TNF against progressing pulmonary metastases. Specifically, the effects of F8-TNF, alone and combined with DOX, on the circulating tumor cells (CTCs), pulmonary metastases, and cells of the immune system were investigated.

Methods

Generation of the K7M2L2 Cell Line

Murine K7 M2 osteosarcoma cells (CRL-2836) were kindly provided by Dr. Chand Khanna (Center for Cancer Research National Institute, Bethesda, MD) and cultured in DMEM (4.5 g/l glucose)/Ham F12 (1:1) medium (Invitrogen, Carlsbad, CA), supplemented with 10% heat-inactivated fetal calf serum (FCS) (GIBCO, Basel, Switzerland), at 37°C in a humidified atmosphere containing 5% CO_2. K7 M2 cells were transduced with a *lacZ* reporter gene under control of a neomycin selection marker as described [25]. Ten microliters of PBS/0.05% EDTA containing 1×10^5 K7 M2/*lacZ* cells were injected into the left tibia [intratibial (i.t.)] of female, 8- to 10-week-old BALB/c mice as described before [25]. The K7M2L2/*lacZ* cell line was obtained after two rounds of *in vivo* selection of pulmonary metastases–derived K7 M2 cells according to Fidler's method [26]. Briefly, around 3 weeks after i.t. injection of K7 M2/*lacZ* cells, mice developed large PTs as well as pulmonary metastases. During sacrifice, the lungs of the mice were collected, and metastasized cells (K7M2L1/lacZ) were isolated by digestion of the lung tissue using collagenase B (Roche, Mannheim, Germany) and subsequently selected in cell culture medium containing 800 μg/ml of G418 (Invitrogen, Life Technologies, Carlsbad, CA). The resulting K7M2L1/*lacZ* cells were then reinjected (i.t.) into BALB/c mice to obtain K7M2L2/*lacZ* cells in the same manner. After *in vivo* selection, K7M2L2/*lacZ* cells were transduced with an *mCherry*-containing plasmid (pQCIXH, containing a hygromycin selection marker), which was kindly provided by Prof. Markus Rudin (Institute of Biomedical Engineering, University and ETH Zurich, Zurich, Switzerland). After transduction, K7M2L2/*lacZ/mCherry* cells were selected in tissue culture medium with 1 mg/ml of G418 (Merck Millipore) and 400 μg/ml of hygromycin (Merck Millipore) to stably express *lacZ* and *mCherry*. A third round of transduction was performed using a pQCIXP plasmid containing the *luciferase2* gene. The original plasmid was kindly provided by Dr. Geertje van der Horst (Leiden University, Leiden, the Netherlands). Ultimately, K7M2L2/*lacZ/mCherry/luciferase2* cells (referred to as "K7M2L2" throughout the manuscript) were selected using growth medium supplemented with 1 mg/ml of G418, 400 μg/ml of hygromycin, and 1 μg/ml of puromycin (Invitrogen).

K7M2L2 Tumor Inductions

Female, 8-week-old BALB/c mice (BALB/cAnNCrl; Charles River Laboratories, Sulzfeld, Germany) were maintained as described [23]. K7M2L2 cells were cultured below confluence, and 1×10^5 K7M2L2 cells were injected into left tibias as described [27]. Upon signs of limping due to the tumor burden, 0.1 mg/kg of intraperitoneal (i.p.) buprenorphine (Temgesic; Reckitt Benckiser, Berkshire, UK) was given twice daily. Body weight measurements were performed weekly. Animal care and experimental procedures were in accordance with the institutional guidelines and approved by the Ethics Committee of the Veterinary Department, Canton of Zurich, Switzerland (license numbers 64/2013 and 160/2015).

Tumor Monitoring and Bone Measurements

After xenografting, tumor growth in the hind limbs of the mice was monitored weekly using caliper measurements as described [28]. To determine tumor load in the lungs or to detect remaining tumor cells at the site of amputation, luciferase activity was measured. Mice were

anesthetized using 5% isoflurane (Forane; AbbVie, Inc., North Chicago, IL), and anesthesia was maintained with 2% isoflurane. XenoLight D-luciferin was injected via the mouse tail vein following the manufacturer's instructions (PerkinElmer, Waltham, MA). Immediately after injection of the substrate, luciferase activity was measured in an IVIS Lumina XR (Caliper Life Sciences, Inc., Hopkinton, MA) and quantified with Living Image v4.4 software (Xenogen Corporation, Alameda, CA).

Micro–computed tomography (microCT) using a SkyScan1176 microCT system (Bruker, Billerica, MA) was performed as described elsewhere [23]. Reconstituted images were segmented using CTAn v1.13.11.0 (Bruker) to select regions of immature bone representing malignant bone formation. Immature bone volumes were determined in a region of interest starting from the distal end of the patella until the convergence of tibia and fibula. Volumes were calculated using the following formula: Δimmature bone volume [mm^3] = bone $volume_{tumor\text{-}limb}$ − bone $volume_{healthy\text{-}limb}$.

Amputations

Amputations were performed under 2% isoflurane anesthesia with preoperative 0.1 mg/kg of i.p. buprenorphine, adapting the procedure described by Wolfe et al. [24]. In brief, the hip region of the tumor-bearing leg was shaved and disinfected with 70% ethanol. A circumferential skin incision was made with small scissors at the plane of the femur/proximal to the PT. After isolating the femoral artery, vein, and nerve (see procedure described in [23]), the femoral artery and vein were concurrently ligated with sterile silk sutures (Fine Science Tools GmbH, Heidelberg, Germany) and cut proximal of the caudal femoral artery. The circumferential musculature was transected distal to the level of vessel ligation and separated from the femur. Using saw-toothed scissors, the femur was then transected proximal to the knee joint at a level which ensured complete macroscopic removal of the PT. Next, the sciatic nerve was identified and transected, followed by the remainder of the ischiocrural musculature to create a flap for subsequent closure. The remaining musculature was used to cover the distal end of the transected femur using 7-0 silk (Braun Melsungen, Melsungen, Germany). The skin was closed using 7-0 silk in an intermittent pattern. After surgery, the animals received 200 µl of 0.9% NaCl i.p. to reestablish physiological fluid levels. Analgesia using 0.1 mg/kg i.p. buprenorphine (Temgesic; Reckitt Benckiser) was continued for 48 hours while closely monitoring the animals, followed by carprofen (Rimadyl; Pfizer, New York, NY; final concentration: 0.067 mg/ml in the drinking water) given *ad libitum* for 5 days [29]. Prior to any treatment study, amputations were first applied in a "pilot amputation study" (See Supplementary methods).

Determination of Amount of Circulating Tumor Cells and Pulmonary Metastases

At necropsy, whole mouse blood was obtained via cardiac puncture. Three healthy, untreated female BALB/c mice served as negative controls. Red blood cell lysis was performed using ammonium-chloride-potassium lysis buffer, and the remaining cells were divided into two parts. One part was briefly centrifuged at 1250 rpm for 3 minutes, dissolved in PBS, and stored at −20°C for the analysis of genomic DNA, whereas the second part was immediately analyzed using fluorescence-activated cell sorting (FACS). Genomic DNA was isolated using a QIAmp DNA blood Mini Kit (Qiagen, Hilden, Germany) following the manufacturer's instructions. Tumor-specific *mCherry*-DNA and glyceraldehyde 3-phosphate dehydrogenase (*GAPDH*)-DNA were amplified using quantitative polymerase chain reaction (PCR) (input: 10 ng of genomic DNA). Primers were purchased from Microsynth (Balgach, Switzerland) and used at 200 nM. Primer sequences are listed in Supplementary Table S1. For quantitative PCR, amplification reactions were carried out using Power SYBR Green PCR master mix (Applied Biosystems, Foster City, CA) and the StepOne Plus Real-Time PCR system (Applied Biosystems). Relative amounts of genomic *mCherry* were determined using the $2^{-\Delta\Delta}$Ct method and normalized to the amount of murine *GAPDH*.

FACS was performed to detect mCherry-positive circulating tumor cells. Following red blood cell lysis of whole blood, cells were suspended in PBS containing 0.5% FCS (Gibco by Thermo Fisher Scientific, Waltham, MA). Fluorescent $mCherry^+$ cells were counted and normalized to the input volume of whole blood using a FACS Aria III cellsorter (BD Biosciences, San Jose, CA). *Postmortem*, X-gal staining of pulmonary metastases of the left lobes of the lung was performed as described [28]. In addition, right lobes of frozen lung were cross sectioned and hematoxylin and eosin stained. A NanoZoomer-XR C12000 (Hamamatsu Photonics K.K., Japan) was used to digitalize the sections, and analysis of metastatic areas was performed using the corresponding NDP.view2 software.

Drug Infusions

The concentration of F8-TNF was adjusted using PBS [19]. Mice anesthetized with 2% isoflurane were kept warm on a heating mat throughout the procedure. Intravenous infusions were performed via the tail vein using a 30G needle attached to a polyethylene catheter (Portex; Smiths Medical, Inc., USA) under control of a syringe pump (Legato; WPI, Inc., USA). Intraarterial infusions were performed similarly as described [23]. Mice received each treatment (PBS or 2 µg of F8-TNF; i.v. or i.a.) every 72 hours for a total of three times. In case of DOX, DOX (5 mg/kg, i.v.; Sandoz, Holzkirchen, Germany) treatment was administered once, as single agent or prior to the first infusion of F8-TNF (i.v.).

Experimental Design

In total, two treatment studies were performed: 1) "comparative treatment study": to compare infusions of i.v. and i.a. F8-TNF (or vehicle = PBS) after establishement of a palpable PT ($n \geq 8$ animals per treatment group; 4 groups) and 2) "combination treatment study": to determine the effect of F8-TNF alone or in combination with DOX on the growth of spontaneous pulmonary metastases and potential local recurrences after amputation of the tumor-bearing hind limb [group "vehicle": $n = 9$; group "F8-TNF": $n = 9$; group "DOX": $n = 8$; group "Comb" (combination; F8-TNF + DOX): $n = 8$]. Three mice did not receive the planned doses and were excluded from all analyses.

Human Osteosarcoma Samples and Ethics Statement

The present study was approved by the local ethics committee (Ref. Nr. EK10/2007), and written informed consent was obtained from each subject or each subject's guardian. Primary human osteosarcoma tissue was stored at −80°C and embedded in Tissue-Tek O.C.T. (Sakura) for sectioning and immunofluorescence.

Immunohistology and Immunofluorescence

At necropsy and after cardiac puncture, mice were perfused with PBS, and PTs and lungs were embedded in Tissue-Tek O.C.T. Compound (Sakura Finetek, USA), frozen on dry ice, and cut (8-10 µm) in a CM3050S cryotome (Leica Biosystems, Newcastle, UK). Frozen tissue sections were fixed in ice-cold acetone, blocked using

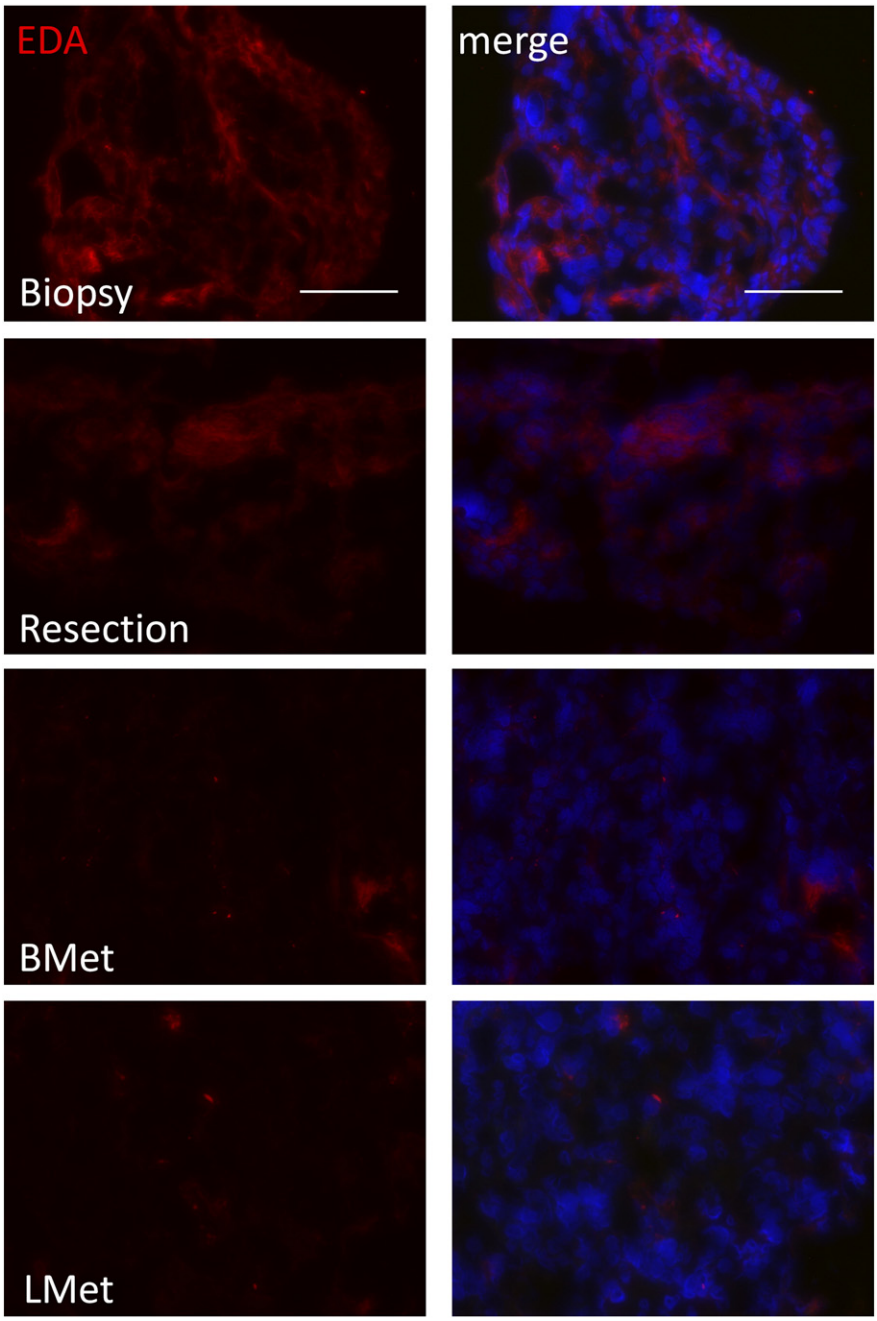

Figure 1. EDA is expressed in various human osteosarcoma tissues. Representative examples of EDA expression (red) in a diagnostic biopsy (before chemotherapy), resection (after chemotherapy), bone metastasis (BMet,) and lung metastasis (LMet). Nuclei were counterstained with Hoechst (blue). EDA staining and merged (EDA and Hoechst) figures are shown separately. Scale bars correspond to 100 μm.

20% FCS (Gibco by Thermo Fisher Scientific) in PBS, and stained. Immunofluorescence was applied on frozen sections to detect EDA (biotinylated F8; 1:100; as described [19]), $CD4^+$ cells (rat anti-CD4, GK1.5; BioXCell, West Lebanon, NH; 1:2000), $CD8^+$ cells (rat anti-CD8a, 2.43, BioXCell; 1:2000), natural killer (NK) cells (rabbit anti-asialo GM1; Wako Pure Chemical Industries, Osaka, Japan; 1:3000), $F4/80^+$ myeloid-derived cells (rat anti-F4/80, CI:A3–1, BioXCell; 1:1000), and $Ly6G^+$ myeloid-derived cells (rat anti-Ly6G, 1A8, BioXCell; 1:2000) using the respective primary antibodies/small immunoproteins diluted in 0.2% BSA (Sigma-Aldrich, St. Louis, MO). Each staining performed also included the respective isotype controls [i.e., a small immunoprotein specific to hen-egg lysozyme (1:150) or IgG2a (rat IgG2a, MAB006, R&D Systems, Minneapolis, MN) or IgG2b (rat IgG2b, LTF-2, BioXCell; 1:2000)]. Primary immunoproteins were detected with streptavidin-coupled Cy-3 (Sigma-Aldrich), goat anti-rabbit IgG-Alexa Fluor 647 (Life Technologies by Thermo Fisher Scientific), goat anti-rabbit IgG-Alexa Fluor 594 (Life Technologies), or goat anti-rat IgG-Alexa Fluor 594 (Life Technologies). Stained slides were mounted with fluorescent Shandon Immu-Mount (Thermo Fisher

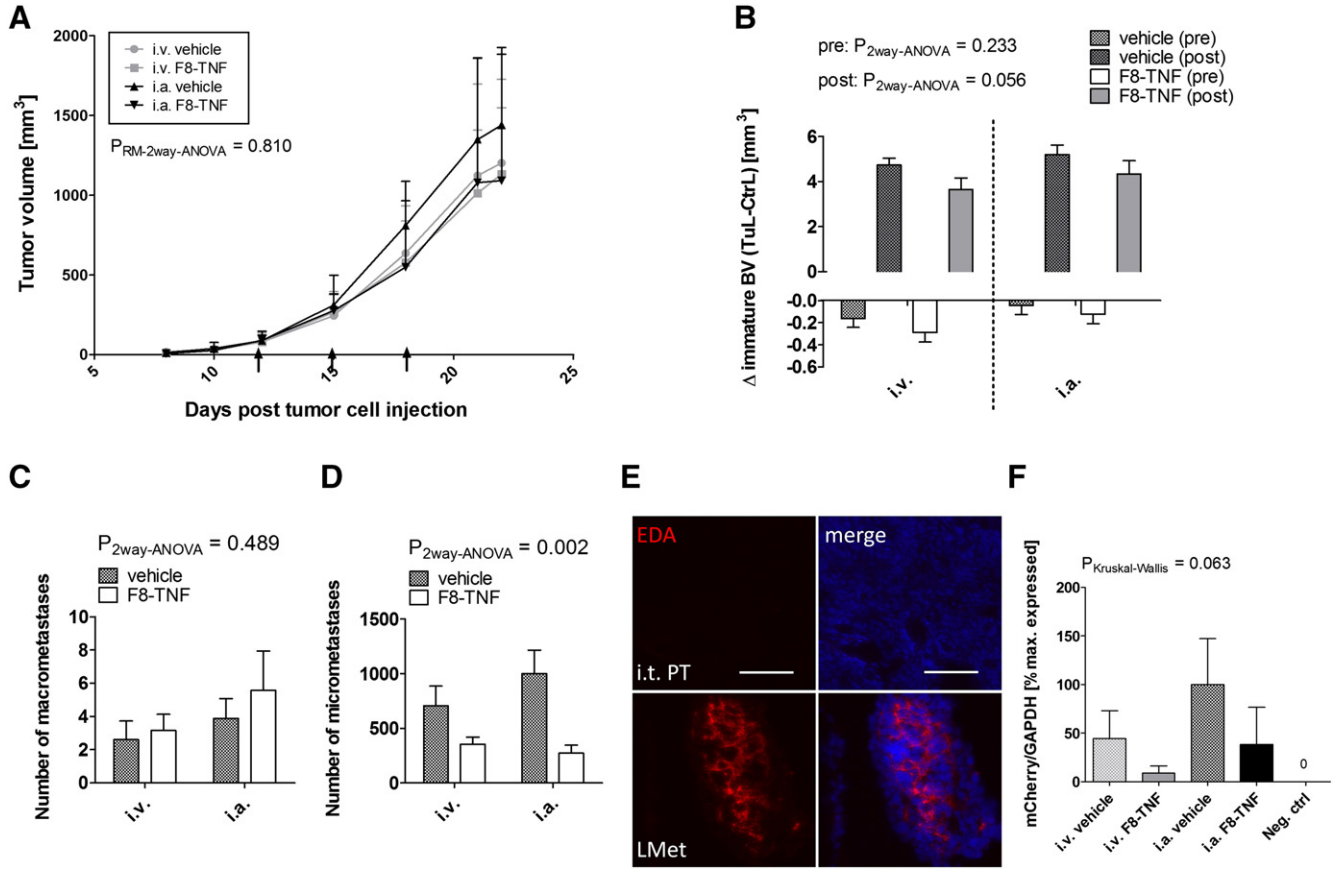

Figure 2. F8-TNF (i.v. and i.a.) has no inhibitory effect on K7M2L2 PT growth yet reduces numbers of early pulmonary metastases. (A) Tumor volumes determined by caliper ($n \geq 8$). Days of drug infusion are indicated by black arrows. (B) Immature bone volumes as determined by microCT scans prior to (pre) and after (post) treatment ($n \geq 8$). Volumes of immature bone were analyzed both in control limbs (CtrL) and in tumor-bearing limbs (TuL). Total number of superficial pulmonary metastases with (C) a diameter >0.5 mm and (D) a diameter <0.5 mm, determined after X-gal staining ($n \geq 5$). (E) Representative sections demonstrate site-dependent EDA (red) expression of K7M2L2 osteosarcoma cells. Nuclei were counterstained with Hoechst (blue). Scale bars correspond to 100 μm. (F) Genomic *mCherry* normalized to *GAPDH* was analyzed using whole blood samples. Highest amount of *mCherry* was set as 100%, and relative values are shown ($n \geq 6$). RM-2way-ANOVA: repeated-measures two-way ANOVA.

Scientific); images were taken with an Axio Observer Z1 (Zeiss, Oberkochen, Germany) and analyzed using ImageJ v1.47 (US National Institutes of Health, Bethesda, MD).

Statistical Analysis

The results were given as mean ± standard error of the mean. Means of end points were compared with one-way or two-way analysis of variance (ANOVA) as indicated, and *P* values of the one-way ANOVA or the column factors (corresponding to treatment, i.e., vehicle versus F8-TNF) were stated in graphs, respectively. In case the data were skewed (skewness >3 as determined by the g1 method), means were analyzed with a Kruskal-Wallis test. In case of one-way ANOVA, Bonferroni posttests were performed to determine statistical differences between individual groups, whereas a Dunn's test was used for skewed data (significant differences were illustrated in graphs). Mean values of time courses were compared with repeated-measures two-way ANOVA unless stated otherwise (*P* values of interactions were stated). Depending on the skewness of the data, Pearson and Spearman correlations were performed. All statistical tests were performed using Prism 5 v5.01 software (GraphPad Software, Inc., La Jolla, CA) and were two-sided, and $P < .05$ was regarded as statistically significant.

Results

EDA Expression in Human Osteosarcoma Tissue

Immunofluorescence against EDA on various samples of primary human osteosarcoma demonstrated the presence of EDA. Briefly, chemotherapy-naïve osteosarcomas (Figure 1; "biopsy"; 5 of 6 EDA$^+$, i.e., 83% of specimens) showed a generally more intense fluorescent staining of EDA yet at a lower frequency compared with chemotherapy-treated ("resection"; 5 of 5; 100%) samples. Metastases present in lungs ("LMet"; 2 of 2; 100%) or bone metastases ("BMet"; 2 of 2; 100%) were EDA positive but yielded weaker staining intensities compared with primary tumors.

Comparative Treatment Study

Effects of F8-TNF Treatment on PT Growth. After confirming the presence of EDA in human osteosarcoma, the effects of F8-TNF against osteosarcoma were evaluated dependent on the route of administration (i.a. versus i.v.) using the orthotopic K7M2L2 osteosarcoma model. After completing three treatments, no significant differences in PT volumes were observed (Figure 2*A*). TNF-α belongs to the class of osteoclastogenic cytokines [30]. To see if F8-TNF treatment impacts bone remodeling, the formation of

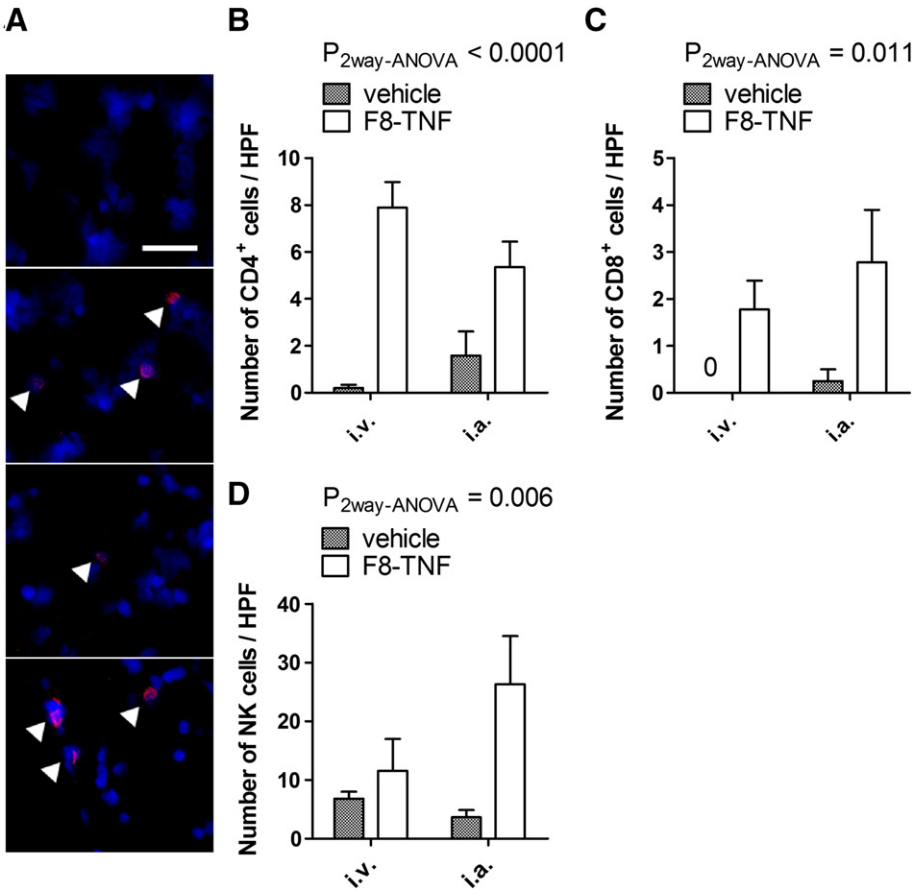

Figure 3. Treatment with F8-TNF increases infiltration of immune cells in the lung. (A) Representative examples of immunofluorescence analysis of $CD4^+$ T cells in the lungs of mice from each treatment group (from top to bottom: i.v. vehicle; i.v. F8-TNF; i.a. vehicle; i.a. F8-TNF). (B) Total numbers of $CD4^+$ ($n \geq 4$), $CD8^+$ [(C), $n \geq 4$], and NK cells [(D), $n \geq 3$] determined in 5 high-power fields (HPF) from lungs of individual mice.

malignant bone tissue during tumor growth was quantified. An increase in tumor-related immature bone production paralleling PT volumes in the K7M2L2 model was observed (Pearson $r = 0.43$, $P = .007$). As expected, no significant difference between immature bone volumes was detected before any treatment (Figure 2*B*). Nevertheless, after F8-TNF treatment, regardless of the route of administration, a trend towards decreased volumes of immature bone deposited by the PTs was detected (Figure 2*B*).

Furthermore, body weights of the mice were recorded to see if the treatment itself impacts the general health of the mice. Throughout the study, no significant differences were observed among the different treatment groups (Supplementary Figure S1*A*). However, because of the tumor growth, a progressing loss of body weight (up to 10% of the initial body weight) was observed. To exclude influences on the downstream blood flow due to the different routes of drug administration used, blood perfusion in the region of tumor growth of the limb was monitored. After three rounds of i.a. or i.v. infusions, no significant differences in perfusion of the region of PT growth were detected (Supplementary Figure S1*B*).

Finally, to confirm the efficacy of the F8-TNF batch used in our experiment, a setup similar to Mortara et al. [31] who demonstrated efficacy of targeted TNF-α against s.c. transplants of K7 M2 osteosarcoma cells was used. Likewise, s.c. transplants of K7M2L2 cells responded to i.v. F8-TNF marked by a reduction in tumor growth and visible hemorrhagic necrosis (Supplementary Figure S2, *A* and *B*). Interestingly, s.c. K7M2L2 transplants were marked by high levels of EDA expression (Supplementary Figure S2*C*).

Reduction of Early Metastatic Growth by F8-TNF. In contrast to the absence of effects of F8-TNF against the PT, a reduction in systemic disease was observed after F8-TNF treatment. Interestingly, dependent on the size of the pulmonary metastases, metastases were differentially affected. Large macrometastases (diameter >0.5 mm; Figure 2*C*) were not affected by either treatment or route of administration, whereas F8-TNF significantly reduced the number of micrometastases (diameter <0.5 mm; Figure 2*D*). At least in part, a stronger expression of EDA by spontaneous pulmonary metastases compared with the corresponding PT might explain the differential effect of F8-TNF (Figure 2*E*).

To see if the reduction in early metastatic outgrowth was also linked to a treatment-dependent reduction in CTCs, the amount of genomic *mCherry* DNA was determined using the cellular fraction of blood samples and qPCR analysis. Treatment with F8-TNF showed a trend towards reduced numbers of CTCs (Figure 2*F*). In addition to qPCR, the amount of CTCs after i.a. F8-TNF was determined using FACS in selected mice. Mice treated with i.a. F8-TNF had reduced numbers of $mCherry^+$ tumor cells within the blood circulation

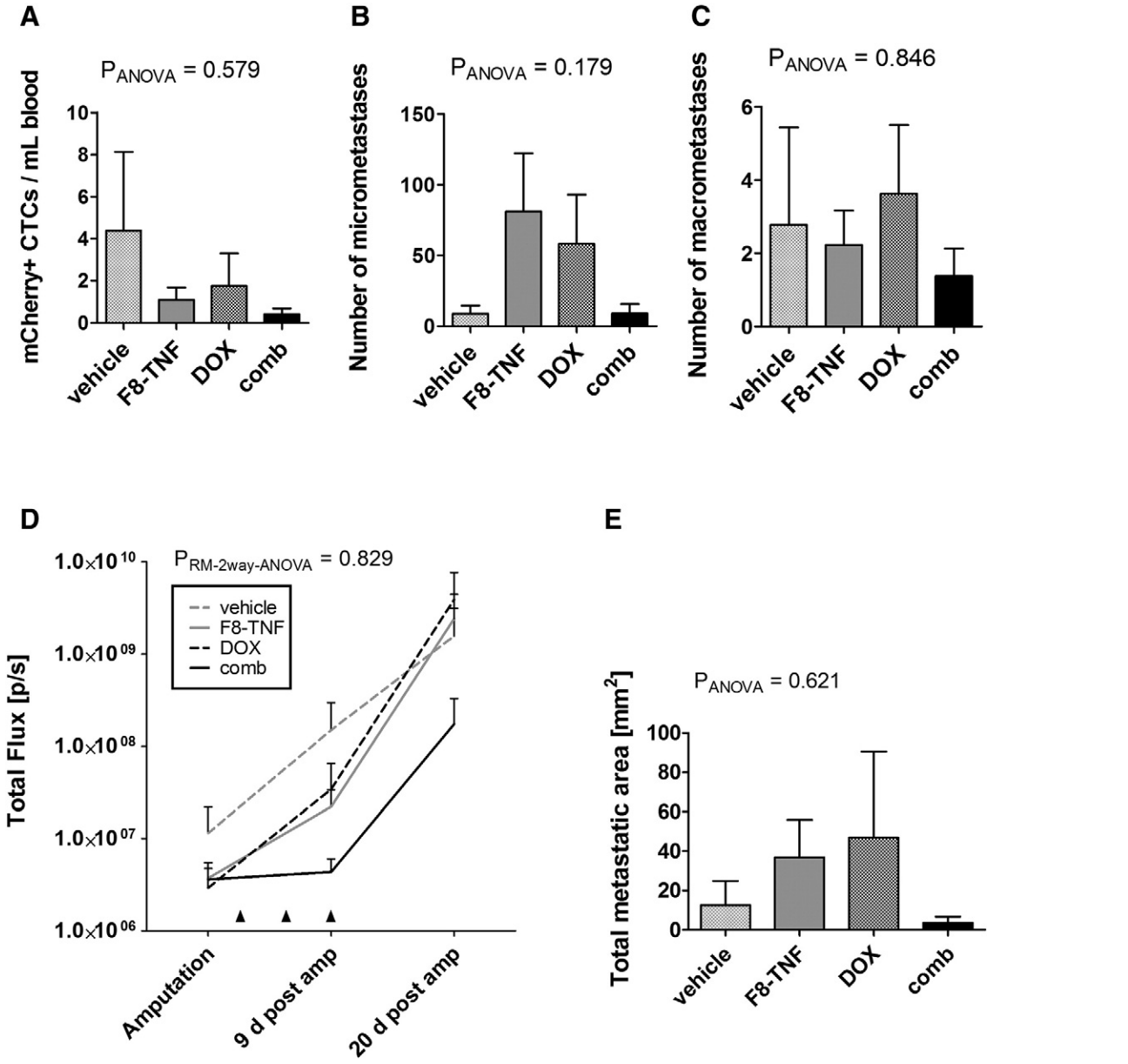

Figure 4. F8-TNF and DOX do not inhibit late metastatic osteosarcoma. (A) CTCs analyzed using FACS of mCherry$^+$ tumor cells detected in whole blood ($n \geq 8$). Quantification of lacZ$^+$ (B) micrometastases (diameter <0.5 mm) and (C) macrometastases (diameter >0.5 mm) detected on the surface of the left lobe of the lung after X-gal staining postmortem ($n \geq 8$). (D) Total area of pulmonary metastases as determined by histological evaluation of lung cross sections ($n \geq 5$). (E) *in vivo* monitoring of luciferase$^+$ tumor cells in the thoracic region by measuring luminescent flux ($n \geq 8$). Black arrowheads indicate administration of treatment. RM-2way-ANOVA: repeated-measures two-way ANOVA; d: days; amp: amputation.

(Supplementary Figure S3). Thus, despite a lack of significant reduction of PT growth, early metastatic disease was affected.

Activation of Immune Cells in the Lung Parenchyma by F8-TNF. Given the role of the immune system in controlling tumor progression, numbers of CD4$^+$ or CD8$^+$ cells and NK cells in the lung parenchyma were quantified using immunofluorescence (e.g., example of CD4$^+$ cells in the lungs depicted in Figure 3*A*). Significantly increased numbers of CD4$^+$ cells (Figure 3*B*) as well as CD8$^+$ cells (Figure 3*C*) in the lung parenchyma were observed after F8-TNF treatment. In case of NK cells (Figure 3*D*), increased numbers were observed after F8-TNF treatment; however, i.a. drug administrations showed a larger increase compared with i.v. administrations.

Combination Treatment Study

F8-TNF Treatment and Progression of Metastases. Next, we tested the efficacy of F8-TNF against late pulmonary metastases in our K7M2L2 model. To this end, a hind limb amputation model was established and characterized. Using this model, we detected a fast recovery of the animals after amputation (Supplementary Figure S4*A*) and found a correlation between increasing numbers of pulmonary metastases and continuous PT growth (Pearson $r = 0.894$; Supplementary Figure S4*B*). Metastatic growth was followed over

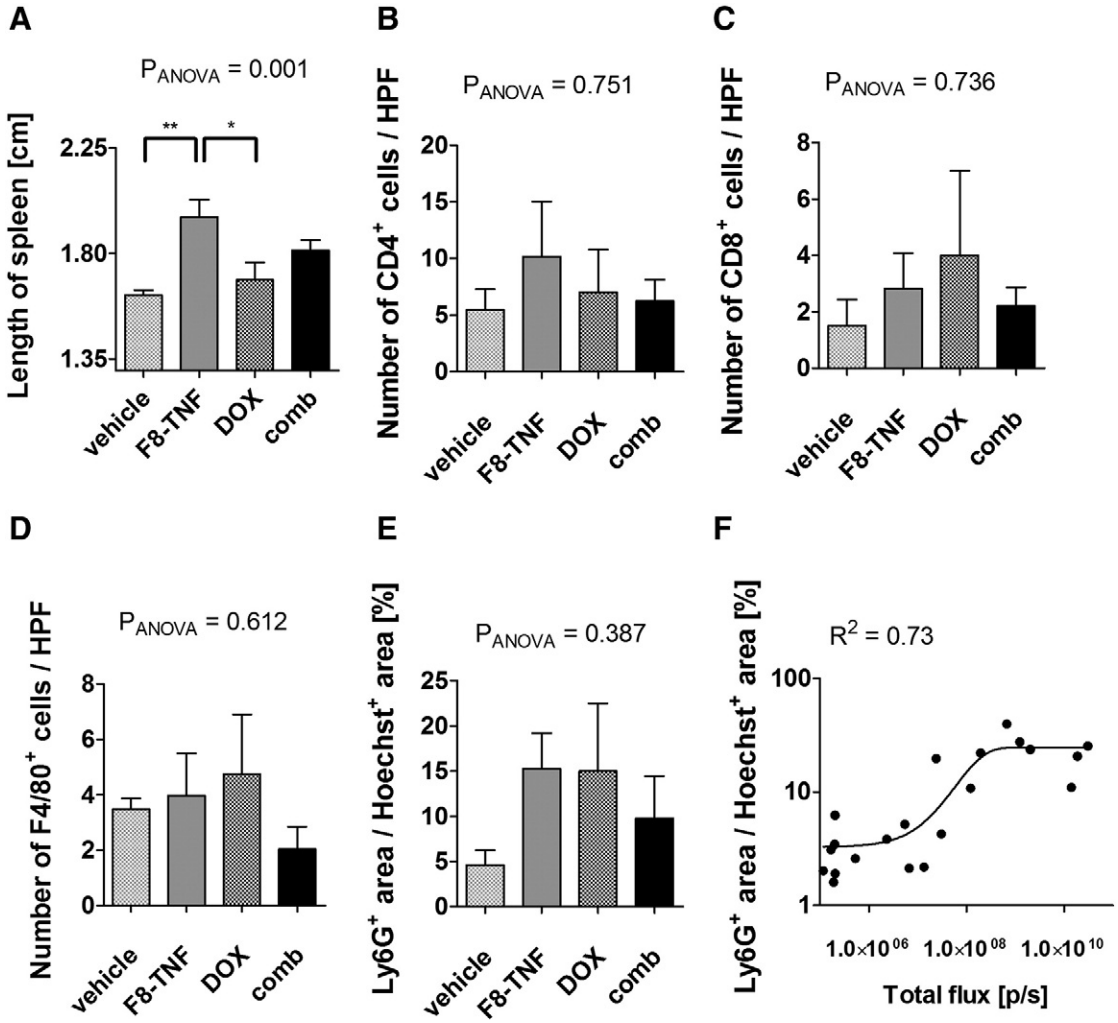

Figure 5. Late metastatic growth associates with pulmonary Ly6G$^+$ myeloid-derived cells. (A) Lengths of spleens were measured *ex vivo* after sacrifice of the mice ($n \geq 8$). (B) Numbers of CD4$^+$ and (C) CD8$^+$ cells as well as (D) F4/80$^+$ myeloid-derived cells in the lungs determined in 5 HPF from lungs of individual mice ($n \geq 5$). (E) Ly6G$^+$ area normalized to the Hoechst$^+$ area in nonmetastatic areas of the lung. Association curve showing a correlation between number of Ly6G$^+$ myeloid-derived cells in the lung parenchyma and growth of luciferase$^+$ pulmonary metastases ($n = 21$).

time (e.g., metastatic growth patterns, Supplementary Figure S4*C* and Supplementary Table S2), yet only amputation of large PT resulted in progression of pulmonary metastases (Supplementary Figure S4*D*). Furthermore, the presence of EDA in progressed metastases was confirmed (Supplementary Figure S4*E*). Moreover, intraabdominal soft tissue recurrences were detected in 33% to 38% of animals which have received limb amputation of a large PT (data not shown).

As shown by Hemmerle et al., DOX, a standard drug also used in osteosarcoma chemotherapy, was shown to potentiate the antitumor effect of F8-TNF [19]. Therefore, we combined the use of DOX and F8-TNF to evaluate the individual and combined efficacies against systemic disease in the context of our amputation model. Similar to the "comparative treatment study," the number of CTCs was evaluated using FACS of mCherry$^+$ tumor cells. However, no significant differences in mean numbers of CTCs were observed (Figure 4*A*). Mice treated with vehicle (range: 0-34 mCherry$^+$ cells/ml) or DOX (0-11) only showed the highest maximum number of CTCs compared with F8-TNF–treated (0–5) or Comb-treated (0–2) animals.

Neither the absolute numbers of X-gal$^+$ micrometastases (Figure 4*B*) nor macrometastases (Figure 4*C*) were significantly affected. Throughout the study, *in vivo* luciferase activity measurements were performed which demonstrated similar progressive growth of late pulmonary metastases in all treatment groups (Figure 4*D*). To validate the *in vivo* measurements, histological determination of metastatic areas in lung cross sections was performed without detecting differences between treatments (Figure 4*E*). However, a significant correlation between luciferase activity in the thoracic region and the histological analysis of total metastatic lung areas was detected (Pearson $r = 0.78$; $P < .0001$). Despite lacking statistical significance, we noticed that the combination treatment indicated the lowest metastatic loads as well as a delay of metastatic growth until the end of the treatment (Figure 4*D*; = "9 d post amp"). In general, all tested treatment regimens were well tolerated without causing a severe loss of body weight (Supplementary Figure S5).

Effects of F8-TNF Treatment on Spleen Size and Numbers of Leukocytes. Enlarged spleens were observed in several immunocompetent mouse models of cancer and were associated with enhanced

metastasis or increased granulocytosis [32–34]. Speculating that F8-TNF treatment might also influence the composition of lymphocytes or granulocytes in our osteosarcoma model, the lengths of spleens were measured. Significantly enlarged spleens were observed after F8-TNF treatment compared with vehicle- or DOX-treated mice (Figure 5*A*). The mean length of spleens of Comb-treated mice was shorter than spleens of F8-TNF–treated mice, without reaching significance. In contrast, the spleen size was not altered after F8-TNF treatment during the "comparative treatment study" (data not shown). Similar to the "comparative treatment" study, we again investigated the immune infiltrate of the lungs. No significant differences between numbers of $CD4^+$ (Figure 5*B*) or $CD8^+$ cells (Figure 5*C*), $F4/80^+$ myeloid-derived cells, or areas of $Ly6G^+$ myeloid-derived cells (Figure 5*D*) in the lung parenchyma were identified. Nevertheless, treatment with F8-TNF tended to increase the mean number of $Ly6G^+$ myeloid-derived cells in the lung parenchyma (15.24 ± 3.96%; percent Ly6G+ myeloid-derived cells ± standard error of the mean) especially if compared with vehicle (4.62 ± 1.66%) but also with DOX (14.99 ± 7.52%) and Comb (9.79 ± 4.66%). In addition, the transition from early (i.e., at the time of amputation) until progressive metastatic growth was closely associated with a stable and significant increase of $Ly6G^+$ myeloid-derived cells in the lung parenchyma irrespective of treatment (Figure 5*E* and Supplementary Figure S6). None of the other immune cells analyzed yielded a similar association (data not shown).

Discussion

In this study, we investigated the effects of targeted TNF-α in early and late stages of osteosarcoma development. We showed that F8-TNF reduced establishment of early micrometastases of osteosarcoma but was not able to significantly prevent the growth of progressing pulmonary metastases. In addition, we demonstrated that the overall efficacy of F8-TNF treatment was largely independent on the route of drug administration (i.a. versus i.v.).

We and others detected the presence of EDA in primary human osteosarcoma tissues, rendering it a potential target for future therapeutic approaches against osteosarcoma [35]. Our results showed a differential expression of EDA in the K7M2L2 osteosarcoma model dependent on the site of tumor growth. Low expression of EDA was observed in orthotopic i.t. PTs, whereas pulmonary metastases derived from their corresponding PT were characterized by stronger EDA expression. Furthermore, s.c. K7M2L2 osteosarcoma transplants were characterized by increased EDA expression compared with i.t. PTs. In addition, F8-TNF treatment of s.c. K7M2L2 transplants resulted in measureable antitumor effects, confirming previously published data [31]. These findings highlight the importance of EDA expression by the target; however, we cannot exclude the possibility that the EDA expression changes with tumor size/stage (e.g., small tumors/metastases might possess higher expression of EDA). Furthermore, reduced efficacy of F8-TNF against i.t. PTs might also be due to the tumor microenvironment (i.e., s.c./skin versus i.t./bone). For instance, the trend in reduced immature bone volume observed after F8-TNF treatment might demonstrate a treatment effect in the vicinity of the tumor (i.e., increased osteoclastogenesis due to local TNF-α [30]), which affects bone remodeling rather than tumor growth. In addition, it is more and more accepted that cells of the bone microenvironment and immune cells are interconnected by a complex cross talk of signaling molecules such as inflammatory cytokines [36]. Nevertheless, further studies are required to fully explain the differences in PT responses after F8-TNF treatment.

It is widely accepted that the establishment of metastasis is a highly selective process. Thus, only a small set of specialized tumor cells is capable of intravasation and distant organ colonization [37], dependent on the expression of specific surface molecules [38–40]. To study the efficacy of an immunomodulatory drug such as F8-TNF, a model recapitulating the establishment of naturally/immune-selected pulmonary metastases is critical. The here presented study used an immunocompetent K7 M2–derived model system which was already considered as being clinically relevant [41]. Through further manipulation of the original K7 M2 cell line, our K7M2L2 model effectively mimicked the different stages of human osteosarcoma progression (i.e., CTCs, development of pulmonary metastases) while at the same time permitting quantitative measurements of each stage. As a limiting factor, the presence of a too large PT is considered as a dropout criterion by our animal welfare agency. Thus, the PT was removed through amputation of the tumor-bearing limb, not only providing longer study times of pulmonary metastases but also being a better representation of clinical progressive metastatic osteosarcoma, where the PT is most frequently removed. In summary, the here described models of spontaneous osteosarcoma metastases allowed the proper assessment of a drug's therapeutic value against metastatic disease [42].

In the "comparative treatment study," a reduction of micrometastatic disease and, thus, action of F8-TNF against early pulmonary metastatic seeds were demonstrated. Recently, other studies demonstrated altered levels of immune cells which were linked to success of therapy against osteosarcoma. For instance, an increase in $CD8^+$ T cells [43] or increases in NK cells [44,45] seemed to be mediators of successful immunotherapy against osteosarcoma and metastases thereof. Likewise, our study demonstrated an increase of $CD4^+$, $CD8^+$, and NK cells in the lung parenchyma after F8-TNF treatment, which may provide an explanation for the reduced numbers of early pulmonary metastases. Especially in the case of i.a. F8-TNF, higher numbers of NK cells in the lung parenchyma were observed, while, at the same time, early micrometastatic seeds were removed more efficiently. In line with our findings, the observation of enhanced removal of early intraluminal metastatic seeds by NK cells in the lung parenchyma [46] might partially explain the efficacy of F8-TNF against early pulmonary metastases. However, further studies will be required to decipher the precise mechanisms of control of early metastatic disease by F8-TNF treatment.

Despite the advantages of studying osteosarcoma in the presence of a PT, a model allowing prolonged study times was required to investigate progressive metastatic disease. Using an amputation model, we demonstrated that progressing pulmonary metastases were not affected by F8-TNF treatment. Even the addition of DOX to F8-TNF only slightly delayed further growth of established metastases. Interestingly, enlarged spleens were observed after F8-TNF therapy yet only in the case of progressive metastatic disease. As demonstrated by others using fibrosarcoma or breast cancer models, enlarged spleens were correlated with increased numbers of myeloid-derived suppressor cells (i.e., monocytes and granulocytes) in general [47] or neutrophils [48], both of which are indicative for an immunosuppressive environment [49]. For instance, production of arginase I by myeloid-derived suppressor cells is considered to be a main mechanism of T cell suppression [50]. In line

with these findings, our study revealed a strong relationship between pulmonary metastatic growth and an increase of $Ly6G^+$ myeloid-derived cells in the lung parenchyma. These observations may suggest the presence of mechanisms invoked by $Ly6G^+$ myeloid-derived cells helping metastasized tumor cells to successfully evade the immune system and continue metastatic outgrowth [51].

Our study showed that targeting of pulmonary metastasis using F8-TNF in osteosarcoma is feasible to reduce early metastatic disease. In contrast, other *in vivo* studies using osteosarcoma cell lines demonstrated an increased metastatic burden if osteosarcoma cells were treated with TNF-α prior to injection [52], whereas the spontaneous metastatic load in an orthotopic model was reduced upon administration of a TNF-α–blocking antibody [53]. These contradicting results might be explained by the use of immunocompromised mice in these studies, where the study of the adaptive immune system was compromised. To our knowledge, no other preclinical studies have assessed the direct effects of targeted TNF-α therapy against osteosarcoma progression so far. In support of our study and TNF-α as a potent anticancer agent, local delivery of TNF-α in immunocompetent models of breast, skin, and lung cancer as well as sarcomas demonstrated strong growth inhibition of PTs [19] and even metastases [54]. However, in contrast to our study, the effects of local delivery of TNF-α on late, spontaneous metastatic growth were not assessed by Dondossola et al. The failure of F8-TNF in reducing progressive metastatic osteosarcoma in our study might be partially explained by a simultaneous increase of $Ly6G^+$ myeloid-derived cells with increasing metastatic burden, similar to what was demonstrated in models of mesothelioma and Lewis lung carcinoma [55]. Here, the targeted delivery of TNF-α to metastatic nodules in the lungs might have provoked an inflammatory reaction which recruited $Ly6G^+$ myeloid-derived cells as the first leukocytes [56]. Likewise, by studying a model of peritonitis, a strong influx of $Ly6G^+$ myeloid-derived cells was observed after local injection of TNF-α [57].

In conclusion, the present study demonstrated efficacy of neoadjuvant F8-TNF against early metastatic disease with minor importance of the route of administration. However, treatment efficacy of F8-TNF against progressive metastatic osteosarcoma was abrogated, seemingly by the presence of an immunosuppressive environment. Taken together, the here presented clinically relevant models of osteosarcoma can be used in future studies to evaluate therapeutic approaches against multiple stages of metastatic osteosarcoma as well as to assess EDA-targeted cytokine delivery to pulmonary metastases.

Appendix A. Supplementary Data

Supplementary data to this article can be found online at http://dx.doi.org/10.1016/j.tranon.2017.02.005.

Authors' Contributions

Conceptualization: B. Robl, S. M. Botter, A. Boro, D. Neri, B. Fuchs.
Methodology: B. Robl, B. Fuchs.
Investigation: B. Robl, S. M. Botter, A. Boro, D. Meier.
Project administration: B. Robl, A. Boro, S. M. Botter.
Writing; original draft preparation: B. Robl.
Writing; review and editing: S. M. Botter, D. Neri, B. Fuchs.
Resources: D. Neri, B. Fuchs.
Supervision: S. M. Botter, D. Neri, B. Fuchs.

Conflict of Interest Disclosure Statement

D. N. is founder and shareholder of Philogen SpA (Siena, Italy), the biotech company that owns the F8 antibody. The remaining authors declare that they have no competing financial or other conflicts of interest.

Acknowledgements

We would like to thank Philipp Probst and Teresa Hemmerle for their technical and administrative support.

References

[1] Mirabello L, Troisi RJ, and Savage SA (2009). Osteosarcoma incidence and survival rates from 1973 to 2004: data from the Surveillance, Epidemiology, and End Results Program. *Cancer* **115**(7), 1531–1543. http://dx.doi.org/10.1002/cncr.24121 [Epub 2009/02/07, PubMed PMID: 19197972; PubMed Central PMCID: PMC2813207].

[2] NA Howlader N, Krapcho M, Garshell J, Neyman N, Altekruse SF, Kosary CL, Yu M, Ruhl J, Tatalovich Z, Cho H, Mariotto A, Lewis DR, Chen HS, Feuer EJ, Cronin KA, editors. Cancer Epidemiology in Older Adolescents and Young Adults 15 to 29 Years of Age, Including SEER Incidence and Survival: 1975-2000. , Institute NC, editor. NIH Pub No 06–5767Bethesda, MD: SEER Cancer Statistics Review, 1975–2010; 2013.

[3] Allison DC, Carney SC, Ahlmann ER, Hendifar A, Chawla S, Fedenko A, Angeles C, and Menendez LR (2012). A meta-analysis of osteosarcoma outcomes in the modern medical era. *Sarcoma* **2012**, 704872. http://dx.doi.org/10.1155/2012/704872 [Epub 2012/05/03, PubMed PMID: 22550423; PubMed Central PMCID: PMC3329715].

[4] Luetke A, Meyers PA, Lewis I, and Juergens H (2014). Osteosarcoma treatment—where do we stand? A state of the art review. *Cancer Treat Rev* **40**(4), 523–532. http://dx.doi.org/10.1016/j.ctrv.2013.11.006 [Epub 2013/12/19, PubMed PMID: 24345772].

[5] Jeys LM, Grimer RJ, Carter SR, Tillman RM, and Abudu A (2007). Post operative infection and increased survival in osteosarcoma patients: are they associated?*Ann Surg Oncol* **14**(10), 2887–2895. http://dx.doi.org/10.1245/s10434-007-9483-8 [Epub 2007/07/27, PubMed PMID: 17653803].

[6] Fritzsching B, Fellenberg J, Moskovszky L, Sápi Z, Krenacs T, Machado I, Poeschl J, Lehner B, Szendrői M, and Bosch AL, et al (2015). CD8/FOXP3-ratio in osteosarcoma microenvironment separates survivors from non-survivors: a multicenter validated retrospective study. *Oncoimmunology* **4**(3), e990800. http://dx.doi.org/10.4161/2162402X.2014.990800 [Epub 2015/05/08, PubMed PMID: 25949908; PubMed Central PMCID: PMC4404826].

[7] Moore C, Eslin D, Levy A, Roberson J, Giusti V, and Sutphin R (2010). Prognostic significance of early lymphocyte recovery in pediatric osteosarcoma. *Pediatr Blood Cancer* **55**(6), 1096–1102. http://dx.doi.org/10.1002/pbc.22673 [Epub 2010/08/25, PubMed PMID: 20734401].

[8] Liu T, Fang XC, Ding Z, Sun ZG, Sun LM, and Wang YL (2015). Pre-operative lymphocyte-to-monocyte ratio as a predictor of overall survival in patients suffering from osteosarcoma. *FEBS Open Bio* **5**, 682–687. http://dx.doi.org/10.1016/j.fob.2015.08.002 [Epub 2015/09/19, PubMed PMID: 26380812; PubMed Central PMCID: PMC4556728].

[9] Meyers PA, Schwartz CL, Krailo MD, Healey JH, Bernstein ML, Betcher D, Ferguson WS, Gebhardt MC, Goorin AM, and Harris M, et al (2008). Osteosarcoma: the addition of muramyl tripeptide to chemotherapy improves overall survival—a report from the Children's Oncology Group. *J Clin Oncol* **26**(4), 633–638. http://dx.doi.org/10.1200/JCO.2008.14.0095 [Epub 2008/02/01, PubMed PMID: 18235123].

[10] Casares N, Pequignot MO, Tesniere A, Ghiringhelli F, Roux S, Chaput N, Schmitt E, Hamai A, Hervas-Stubbs S, and Obeid M, et al (2005). Caspase-dependent immunogenicity of doxorubicin-induced tumor cell death. *J Exp Med* **202**(12), 1691–1701. http://dx.doi.org/10.1084/jem.20050915 [Epub 2005/12/21, PubMed PMID: 16365148; PubMed Central PMCID: PMC2212968].

[11] Carswell EA, Old LJ, Kassel RL, Green S, Fiore N, and Williamson B (1975). An endotoxin-induced serum factor that causes necrosis of tumors. *Proc Natl Acad Sci U S A* **72**(9), 3666–3670 [Epub 1975/09/01, PubMed PMID: 1103152; PubMed Central PMCID: PMC433057].

[12] Wiemann B and Starnes CO (1994). Coley's toxins, tumor necrosis factor and cancer research: a historical perspective. *Pharmacol Ther* **64**(3), 529–564 [Epub 1994/01/01, PubMed PMID: 7724661].

[13] Gasparri A, Moro M, Curnis F, Sacchi A, Pagano S, Veglia F, Casorati G, Siccardi AG, Dellabona P, and Corti A (1999). Tumor pretargeting with avidin improves the therapeutic index of biotinylated tumor necrosis factor alpha in mouse models. *Cancer Res* **59**(12), 2917–2923 [Epub 1999/06/26, PubMed PMID: 10383155].

[14] Palladino Jr MA, Shalaby MR, Kramer SM, Ferraiolo BL, Baughman RA, Deleo AB, Crase D, Marafino B, Aggarwal BB, and Figari IS, et al (1987). Characterization of the antitumor activities of human tumor necrosis factor-alpha and the comparison with other cytokines: induction of tumor-specific immunity. *J Immunol* **138**(11), 4023–4032 [Epub 1987/06/01, PubMed PMID: 3295044].

[15] Havell EA, Fiers W, and North RJ (1988). The antitumor function of tumor necrosis factor (TNF), I. Therapeutic action of TNF against an established murine sarcoma is indirect, immunologically dependent, and limited by severe toxicity. *J Exp Med* **167**(3), 1067–1085 [Epub 1988/03/01, PubMed PMID: 3351434; PubMed Central PMCID: PMC2188888].

[16] Eggermont AM, Schraffordt Koops H, Liénard D, Kroon BB, van Geel AN, Hoekstra HJ, and Lejeune FJ (1996). Isolated limb perfusion with high-dose tumor necrosis factor-alpha in combination with interferon-gamma and melphalan for nonresectable extremity soft tissue sarcomas: a multicenter trial. *J Clin Oncol* **14**(10), 2653–2665 [Epub 1996/10/01, PubMed PMID: 8874324].

[17] Tracey KJ and Cerami A (1994). Tumor necrosis factor: a pleiotropic cytokine and therapeutic target. *Annu Rev Med* **45**, 491–503. http://dx.doi.org/10.1146/annurev.med.45.1.491 [Epub 1994/01/01, PubMed PMID: 8198398].

[18] Borsi L, Balza E, Carnemolla B, Sassi F, Castellani P, Berndt A, Kosmehl H, Biro A, Siri A, and Orecchia P, et al (2003). Selective targeted delivery of TNFalpha to tumor blood vessels. *Blood* **102**(13), 4384–4392. http://dx.doi.org/10.1182/-blood-2003-04-1039 [Epub 2003/08/23, PubMed PMID: 12933583].

[19] Hemmerle T, Probst P, Giovannoni L, Green AJ, Meyer T, and Neri D (2013). The antibody-based targeted delivery of TNF in combination with doxorubicin eradicates sarcomas in mice and confers protective immunity. *Br J Cancer* **109**(5), 1206–1213. http://dx.doi.org/10.1038/bjc.2013.421 [Epub 2013/07/28, PubMed PMID: 23887603; PubMed Central PMCID: PMC3778281].

[20] Curnis F, Sacchi A, Borgna L, Magni F, Gasparri A, and Corti A (2000). Enhancement of tumor necrosis factor alpha antitumor immunotherapeutic properties by targeted delivery to aminopeptidase N (CD13). *Nat Biotechnol* **18**(11), 1185–1190. http://dx.doi.org/10.1038/81183 [Epub 2000/11/04, PubMed PMID: 11062439].

[21] Lu L, Li ZJ, Li LF, Wu WK, Shen J, Zhang L, Chan RL, Yu L, Liu YW, and Ren SX, et al (2015). Vascular-targeted TNFalpha improves tumor blood vessel function and enhances antitumor immunity and chemotherapy in colorectal cancer. *J Control Release* **210**, 134–146. http://dx.doi.org/10.1016/j.jconrel.2015.05.282 [Epub 2015/05/25, PubMed PMID: 26003042].

[22] Jaffe N, Knapp J, Chuang VP, Wallace S, Ayala A, Murray J, Cangir A, Wang A, and Benjamin RS (1983). Osteosarcoma: intra-arterial treatment of the primary tumor with cis-diammine-dichloroplatinum II (CDP). Angiographic, pathologic, and pharmacologic studies. *Cancer* **51**(3), 402–407 [Epub 1983/02/01, PubMed PMID: 6571796].

[23] Robl B, Botter SM, Pellegrini G, Neklyudova O, and Fuchs B (2016). Evaluation of intraarterial and intravenous cisplatin chemotherapy in the treatment of metastatic osteosarcoma using an orthotopic xenograft mouse model. *J Exp Clin Cancer Res* **35**(1), 113. http://dx.doi.org/10.1186/s13046-016-0392-1 [Epub 2016/07/17, PubMed PMID: 27421768].

[24] Wolfe TD, Pillai SP, Hildreth III BE, Lanigan LG, Martin CK, Werbeck JL, and Rosol TJ (2011). Effect of zoledronic acid and amputation on bone invasion and lung metastasis of canine osteosarcoma in nude mice. *Clin Exp Metastasis* **28**(4), 377–389. http://dx.doi.org/10.1007/s10585-011-9377-9 [Epub 2011/03/05, PubMed PMID: 21374084; PubMed Central PMCID: PMC4284437].

[25] Sabile AA, Arlt MJ, Muff R, Bode B, Langsam B, Bertz J, Jentzsch T, Puskas GJ, Born W, and Fuchs B (2011). Cyr61 expression in Osteosarcoma indicates poor prognosis and promotes intratibial growth and lung metastasis in mice. *J Bone Miner Res*. http://dx.doi.org/10.1002/jbmr.535 [Epub 2011/10/07, PubMed PMID: 21976359].

[26] Fidler IJ, Naito S, and Pathak S (1990). Orthotopic implantation is essential for the selection, growth and metastasis of human renal cell cancer in nude mice [corrected]. *Cancer Metastasis Rev* **9**(2), 149–165 [Epub 1990/09/01, PubMed PMID: 2253314].

[27] Husmann K, Arlt MJ, Jirkof P, Arras M, Born W, and Fuchs B (2015). Primary tumour growth in an orthotopic osteosarcoma mouse model is not influenced by analgesic treatment with buprenorphine and meloxicam. *Lab Anim* **49**(4), 284–293. http://dx.doi.org/10.1177/0023677215570989 [Epub 2015/02/05, PubMed PMID: 25650386].

[28] Arlt MJ, Banke IJ, Walters DK, Puskas GJ, Steinmann P, Muff R, Born W, and Fuchs B (2011). LacZ transgene expression in the subcutaneous Dunn/LM8 osteosarcoma mouse model allows for the identification of micrometastasis. *J Orthop Res* **29**(6), 938–946. http://dx.doi.org/10.1002/jor.21304 [Epub 2011/02/02, PubMed PMID: 21284029].

[29] Ingrao JC, Johnson R, Tor E, Gu Y, Litman M, and Turner PV (2013). Aqueous stability and oral pharmacokinetics of meloxicam and carprofen in male C57BL/6 mice. *J Am Assoc Lab Anim Sci* **52**(5), 553–559 [Epub 2013/09/18, PubMed PMID: 24041210; PubMed Central PMCID: PMC3784660].

[30] Nakashima T, Kobayashi Y, Yamasaki S, Kawakami A, Eguchi K, Sasaki H, and Sakai H (2000). Protein expression and functional difference of membrane-bound and soluble receptor activator of NF-kappaB ligand: modulation of the expression by osteotropic factors and cytokines. *Biochem Biophys Res Commun* **275**(3), 768–775. http://dx.doi.org/10.1006/bbrc.2000.3379 [Epub 2000/09/07, PubMed PMID: 10973797].

[31] Mortara L, Orecchia P, Castellani P, Borsi L, Carnemolla B, and Balza E (2013). Schedule-dependent therapeutic efficacy of L19mTNF-alpha and melphalan combined with gemcitabine. *Cancer Med* **2**(4), 478–487. http://dx.doi.org/10.1002/cam4.89 [Epub 2013/10/25, PubMed PMID: 24156020; PubMed Central PMCID: PMC3799282].

[32] Cao M, Xu Y, Youn JI, Cabrera R, Zhang X, Gabrilovich D, Nelson DR, and Liu C (2011). Kinase inhibitor sorafenib modulates immunosuppressive cell populations in a murine liver cancer model. *Lab Invest* **91**(4), 598–608. http://dx.doi.org/10.1038/labinvest.2010.205 [Epub 2011/02/16, PubMed PMID: 21321535; PubMed Central PMCID: PMC3711234].

[33] DuPre SA and Hunter Jr KW (2007). Murine mammary carcinoma 4T1 induces a leukemoid reaction with splenomegaly: association with tumor-derived growth factors. *Exp Mol Pathol* **82**(1), 12–24. http://dx.doi.org/10.1016/j.yexmp.2006.06.007 [Epub 2006/08/22, PubMed PMID: 16919266].

[34] Sato N, Michaelides MC, and Wallack MK (1981). Characterization of tumorigenicity, mortality, metastasis, and splenomegaly of two cultured murine colon lines. *Cancer Res* **41**(6), 2267–2272 [Epub 1981/06/01, PubMed PMID: 7237427].

[35] Kilian O, Dahse R, Alt V, Zardi L, Rosenhahn J, Exner U, Battmann A, Schnettler R, and Kosmehl H (2004). Expression of EDA+ and EDB+ fibronectin splice variants in bone. *Bone* **35**(6), 1334–1345. http://dx.doi.org/10.1016/j.bone.2004.08.008 [Epub 2004/12/14, PubMed PMID: 15589214].

[36] Criscitiello C, Viale G, Gelao L, Esposito A, De Laurentiis M, De Placido S, Santangelo M, Goldhirsch A, and Curigliano G (2015). Crosstalk between bone niche and immune system: osteoimmunology signaling as a potential target for cancer treatment. *Cancer Treat Rev* **41**(2), 61–68. http://dx.doi.org/10.1016/j.ctrv.2014.12.001 [Epub 2014/12/17, PubMed PMID: 25499997].

[37] Valastyan S and Weinberg RA (2011). Tumor metastasis: molecular insights and evolving paradigms. *Cell* **147**(2), 275–292. http://dx.doi.org/10.1016/j.cell.2011.09.024 [Epub 2011/10/18, PubMed PMID: 22000009; PubMed Central PMCID: PMC3261217].

[38] Steinert G, Schölch S, Niemietz T, Iwata N, García SA, Behrens B, Voigt A, Kloor M, Benner A, and Bork U, et al (2014). Immune escape and survival mechanisms in circulating tumor cells of colorectal cancer. *Cancer Res* **74**(6), 1694–1704. http://dx.doi.org/10.1158/0008-5472.CAN-13-1885 [Epub 2014/03/07, PubMed PMID: 24599131].

[39] Xu JF, Pan XH, Zhang SJ, Zhao C, Qiu BS, Gu HF, Hong JF, Cao L, Chen Y, and Xia B, et al (2015). CD47 blockade inhibits tumor progression human osteosarcoma in xenograft models. *Oncotarget* **6**(27), 23662–23670. http://dx.doi.org/10.18632/oncotarget.4282 [Epub 2015/06/21, PubMed PMID: 26093091; PubMed Central PMCID: PMC4695143].

[40] Koshkina NV, Khanna C, Mendoza A, Guan H, DeLauter L, and Kleinerman ES (2007). Fas-negative osteosarcoma tumor cells are selected during metastasis to the lungs: the role of the Fas pathway in the metastatic process of osteosarcoma. *Mol Cancer Res* **5**(10), 991–999. http://dx.doi.org/10.1158/1541-7786.MCR-07-0007 [Epub 2007/10/24, PubMed PMID: 17951400].

[41] Khanna C, Prehn J, Yeung C, Caylor J, Tsokos M, and Helman L (2000). An orthotopic model of murine osteosarcoma with clonally related variants differing in pulmonary metastatic potential. *Clin Exp Metastasis* **18**(3), 261–271 [Epub 2001/04/21, PubMed PMID: 11315100].

[42] Khanna C, Fan TM, Gorlick R, Helman LJ, Kleinerman ES, Adamson PC, Houghton PJ, Tap WD, Welch DR, and Steeg PS, et al (2014). Toward a drug development path that targets metastatic progression in osteosarcoma. *Clin Cancer Res* **20**(16), 4200–4209. http://dx.doi.org/10.1158/1078-0432.CCR-13-2574 [Epub 2014/05/08, PubMed PMID: 24803583; PubMed Central PMCID: PMC4134738].

[43] Yu Z, Geng J, Zhang M, Zhou Y, Fan Q, and Chen J (2014). Treatment of osteosarcoma with microwave thermal ablation to induce immunogenic cell death. *Oncotarget* **5**(15), 6526–6539. http://dx.doi.org/10.18632/oncotarget.2310 [Epub 2014/08/26, PubMed PMID: 25153727; PubMed Central PMCID: PMC4171648].

[44] Fernandez L, Valentin J, Zalacain M, Leung W, Patino-Garcia A, and Perez-Martinez A (2015). Activated and expanded natural killer cells target osteosarcoma tumor initiating cells in an NKG2D-NKG2DL dependent manner. *Cancer Lett* **368**(1), 54–63. http://dx.doi.org/10.1016/j.canlet.2015.07.042 [Epub 2015/08/16, PubMed PMID: 26276724].

[45] Guma SR, Lee DA, Yu L, Gordon N, Hughes D, Stewart J, Wang WL, and Kleinerman ES (2014). Natural killer cell therapy and aerosol interleukin-2 for the treatment of osteosarcoma lung metastasis. *Pediatr Blood Cancer* **61**(4), 618–626. http://dx.doi.org/10.1002/pbc.24801 [Epub 2013/10/19, PubMed PMID: 24136885; PubMed Central PMCID: PMC4154381].

[46] Spiegel A, Brooks MW, Houshyar S, Reinhardt F, Ardolino M, Fessler E, Chen MB, Krall JA, DeCock J, and Zervantonakis IK, et al (2016). Neutrophils suppress intraluminal NK cell–mediated tumor cell clearance and enhance extravasation of disseminated carcinoma cells. *Cancer Discov* **6**(6), 630–649. http://dx.doi.org/10.1158/2159-8290.CD-15-1157 [Epub 2016/04/14, PubMed PMID: 27072748; PubMed Central PMCID: PMC4918202].

[47] Marigo I, Bosio E, Solito S, Mesa C, Fernandez A, Dolcetti L, Ugel S, Sonda N, Bicciato S, and Falisi E, et al (2010). Tumor-induced tolerance and immune suppression depend on the C/EBPbeta transcription factor. *Immunity* **32**(6), 790–802. http://dx.doi.org/10.1016/j.immuni.2010.05.010 [Epub 2010/07/08, PubMed PMID: 20605485].

[48] Coffelt SB, Kersten K, Doornebal CW, Weiden J, Vrijland K, Hau CS, Verstegen NJ, Ciampricotti M, Hawinkels LJ, and Jonkers J, et al (2015). IL-17-producing gammadelta T cells and neutrophils conspire to promote breast cancer metastasis. *Nature* **522**(7556), 345–348. http://dx.doi.org/10.1038/nature14282 [Epub 2015/03/31, PubMed PMID: 25822788; PubMed Central PMCID: PMC4475637].

[49] Cortez-Retamozo V, Etzrodt M, Newton A, Rauch PJ, Chudnovskiy A, Berger C, Ryan RJ, Iwamoto Y, Marinelli B, and Gorbatov R, et al (2012). Origins of tumor-associated macrophages and neutrophils. *Proc Natl Acad Sci U S A* **109**(7), 2491–2496. http://dx.doi.org/10.1073/pnas.1113744109 [Epub 2012/02/07, PubMed PMID: 22308361; PubMed Central PMCID: PMC3289379].

[50] Rodriguez PC and Ochoa AC (2008). Arginine regulation by myeloid derived suppressor cells and tolerance in cancer: mechanisms and therapeutic perspectives. *Immunol Rev* **222**, 180–191. http://dx.doi.org/10.1111/j.1600-065X.2008.00608.x [Epub 2008/03/28, PubMed PMID: 18364002; PubMed Central PMCID: PMC3546504].

[51] Tuting T and de Visser KE (2016). CANCER. How neutrophils promote metastasis. *Science* **352**(6282), 145–146. http://dx.doi.org/10.1126/science.aaf7300 [Epub 2016/04/29, PubMed PMID: 27124439].

[52] Kawashima A, Nakanishi I, Tsuchiya H, Roessner A, Obata K, and Okada Y (1994). Expression of matrix metalloproteinase 9 (92-kDa gelatinase/type IV collagenase) induced by tumour necrosis factor alpha correlates with metastatic ability in a human osteosarcoma cell line. *Virchows Arch* **424**(5), 547–552 [Epub 1994/01/01, PubMed PMID: 8032535].

[53] Kato H, Wakabayashi H, Naito Y, Kato S, Nakagawa T, Matsumine A, and Sudo A (2015). Anti-tumor necrosis factor therapy inhibits lung metastasis in an osteosarcoma cell line. *Oncology* **88**(3), 139–146. http://dx.doi.org/10.1159/000368414 [Epub 2014/11/18, PubMed PMID: 25402182].

[54] Dondossola E, Dobroff AS, Marchiò S, Cardó-Vila M, Hosoya H, Libutti SK, Corti A, Sidman RL, Arap W, and Pasqualini R (2016). Self-targeting of TNF-releasing cancer cells in preclinical models of primary and metastatic tumors. *Proc Natl Acad Sci U S A* **113**(8), 2223–2228. http://dx.doi.org/10.1073/pnas.1525697113 [Epub 2016/02/10, PubMed PMID: 26858439].

[55] Mishalian I, Bayuh R, Levy L, Zolotarov L, Michaeli J, and Fridlender ZG (2013). Tumor-associated neutrophils (TAN) develop pro-tumorigenic properties during tumor progression. *Cancer Immunol Immunother* **62**(11), 1745–1756. http://dx.doi.org/10.1007/s00262-013-1476-9 [Epub 2013/10/05, PubMed PMID: 24092389].

[56] Kolaczkowska E and Kubes P (2013). Neutrophil recruitment and function in health and inflammation. *Nat Rev Immunol* **13**(3), 159–175. http://dx.doi.org/10.1038/nri3399 [Epub 2013/02/26, PubMed PMID: 23435331].

[57] Buscher K, Wang H, Zhang X, Striewski P, Wirth B, Saggu G, Lütke-Enking S, Mayadas TN, Ley K, and Sorokin L, et al (2016). Protection from septic peritonitis by rapid neutrophil recruitment through omental high endothelial venules. *Nat Commun* **7**, 10828. http://dx.doi.org/10.1038/ncomms10828 [Epub 2016/03/05, PubMed PMID: 26940548; PubMed Central PMCID: PMC4785224].